molecular pharmaceutics

Subscriber access provided by UNIV OF CAMBRIDGE

Article

Development and Evaluation of an 18F-Radiolabeled Monocyclam Derivative for Imaging CXCR4 Expression

Diana Brickute, Marta Braga, Maciej A. Kaliszczak, Chris Barnes, Doreen Lau, Laurence Carroll, Elizabeth Stevens, Sebastian Trousil, Israt S. Alam, Quang-De Nguyen, and Eric O. Aboagye

Mol. Pharmaceutics, **Just Accepted Manuscript** • DOI: 10.1021/acs.molpharmaceut.9b00069 • Publication Date (Web): 18 Mar 2019

Downloaded from http://pubs.acs.org on March 19, 2019

Just Accepted

"Just Accepted" manuscripts have been peer-reviewed and accepted for publication. They are posted online prior to technical editing, formatting for publication and author proofing. The American Chemical Society provides "Just Accepted" as a service to the research community to expedite the dissemination of scientific material as soon as possible after acceptance. "Just Accepted" manuscripts appear in full in PDF format accompanied by an HTML abstract. "Just Accepted" manuscripts have been fully peer reviewed, but should not be considered the official version of record. They are citable by the Digital Object Identifier (DOI®). "Just Accepted" is an optional service offered to authors. Therefore, the "Just Accepted" Web site may not include all articles that will be published in the journal. After a manuscript is technically edited and formatted, it will be removed from the "Just Accepted" Web site and published as an ASAP article. Note that technical editing may introduce minor changes to the manuscript text and/or graphics which could affect content, and all legal disclaimers and ethical guidelines that apply to the journal pertain. ACS cannot be held responsible for errors or consequences arising from the use of information contained in these "Just Accepted" manuscripts.

ACS Publications

is published by the American Chemical Society. 1155 Sixteenth Street N.W., Washington, DC 20036

Published by American Chemical Society. Copyright © American Chemical Society. However, no copyright claim is made to original U.S. Government works, or works produced by employees of any Commonwealth realm Crown government in the course of their duties.

Development and Evaluation of an ^{18}F-Radiolabeled Monocyclam Derivative for Imaging CXCR4 Expression

Diana Brickute,[a,†] Marta Braga,[a,†] Maciej A. Kaliszczak,[a] Chris Barnes,[a] Doreen Lau,[a] Laurence Carroll,[a] Elizabeth Stevens,[a] Sebastian Trousil,[a] Israt S. Alam,[a] Quang-Dé Nguyen [a] and Eric O. Aboagye[a]*

[a] Cancer Imaging Centre, Department of Surgery and Cancer, Imperial College London, Faculty of Medicine, Hammersmith Hospital Campus, Du Cane Road, London W12 0NN, United Kingdom.

[†] These authors contributed equally to this work.

Keywords: CXCR4, Cyclam, [^{18}F]MCFB, AMD3465

ABSTRACT

C-X-C chemokine receptor type 4 (CXCR4) is a protein that in humans is encoded by the *CXCR4* gene and binds the ligand CXCL12 (also known as SDF-1). The CXCR4-CXCL12 interaction in cancer elicits biological activities that result in tumor progression and has accordingly been the subject of significant investigation for detection and treatment of disease. Peptidic antagonists have been labeled with a variety of radioisotopes for detection of CXCR4, but methodology utilizing small molecules have predominantly used radiometals. We report here the development of a ^{18}F-radiolabeled cyclam-based small molecule radioprobe, [^{18}F]MCFB, for imaging CXCR4 expression. The IC_{50} of [^{19}F]MCFB for CXCR4 was similar to that of AMD3465 (111.3 and 89.9 nM, respectively). *In vitro* binding assays show that the tracer depicted differential CXCR4 expression, which was blocked in the presence of AMD3465, demonstrating specificity of [^{18}F]MCFB. Positron emission tomography (PET) imaging studies showed distinct uptake of radioprobe in lymphoma and breast cancer xenografts. High liver and kidney uptake were seen with [^{18}F]MCFB leading us to further examine the basis of its pharmacokinetics in relation to the tracer's cationic nature, thus, the role of organic cation transporters (OCTs). Substrate competition following the intravenous injection of metformin led to a marked decrease in urinary excretion of [^{18}F]MCFB, with moderate changes observed in other organs, including the liver. Our results suggest involvement of OCTs in renal elimination of the tracer. In conclusion, the ^{18}F radiolabeled monocyclam, [^{18}F]MCFB, has potential to detect tumor CXCR4 in non-hepatic tissue.

INTRODUCTION

C-X-C chemokine receptor type 4 (CXCR4) is a seven-transmembrane domain G protein-coupled receptor that in humans is encoded by the CXCR4 gene. Binding of CXCR4 to its cognate ligand, CXCL12 (also known as SDF-1), leads to the activation of several downstream signaling pathways that control cellular responses including proliferation, survival, chemotaxis and transcription.[1,2] These CXCR4-regulated pathways exert critical functions in development and normal physiology, as well as in disease processes. In fact, CXCR4 upregulation has been reported in over 20 types of malignant cancers and is correlated with poor prognosis and an aggressive phenotype. Organ-specific metastatic spread, for instance, has been attributed in part to CXCR4-CXCL12 interaction,[3,4] wherein CXCR4 expressing tumor cells migrate to CXCL12-rich environments such as lymph nodes, lung, liver, and bone marrow. Along with metastatic spread, the CXCR4-CXCL12 axis impact other aspects of tumor progression, including provision of a protective niche for tumor cells in the bone marrow and supporting hypoxia-driven angiogenesis through recruitment of CXCR4-positive pro-angiogenic cells.[5,6]

Increased understanding of the pivotal role of CXCR4 in tumor biology has resulted in the development of imaging probes that can provide sensitive and rapid detection of CXCR4 expression. Positron emission tomography (PET) is a sensitive nuclear functional imaging modality used frequently in oncology for diagnosis, staging and monitoring treatment response. The development of novel PET imaging agents to target receptors that are characteristic of malignant phenotype is an important area of research and strives towards personalized medicine. CXCR4 is an attractive target for

developing PET radioligands because of its role and overexpression in some cancers and other diseases. One of the most studied classes of CXCR4 imaging agents comprise of peptidic radioprobes; screening of molecules against HIV infection led to the discovery of T140, a 14-residue peptide with a disulphide bridge that has been functionalized with various chelators/radionuclides for CXCR4 detection.[7–9] Cyclopentapeptides have also been used for the development of new imaging tracers. An important milestone in CXCR4 imaging was achieved by Demmer et al, in developing a ^{68}Ga-labeled cyclopentapeptide, [^{68}Ga]CPCR4-2 ([^{68}Ga]Pentixafor), that has reached clinical trials due to its persistent tumor accumulation and favorable pharmacokinetics.[10,11]

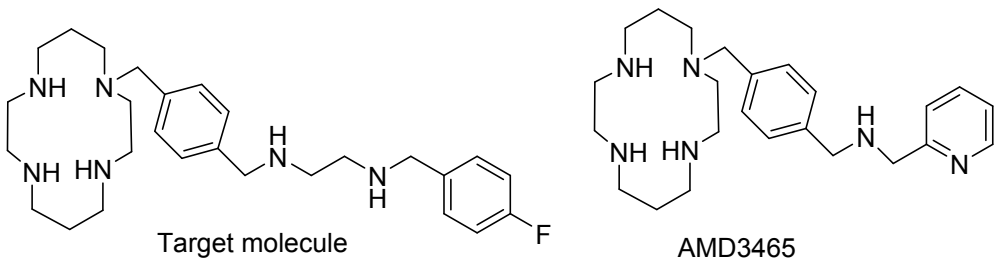

Figure 1. Chemical structures of the target molecule (MCFB or compound **5**) and AMD3465.

An extensive array of small molecule CXCR4 antagonists covering over 20 different chemical classes of compounds have been developed and discussed;[12] however, their application to imaging has been limited. The cyclam AMD3465 (**Figure 1**) and bicyclam AMD3100 currently represent the most studied class of non-peptide CXCR4 inhibitors for nuclear imaging, predominantly PET. The metal-chelating properties of cyclams have been used to radiolabel both AMD3100 and AMD3465 with ^{64}Cu.[13–16] While both compounds gave significant tumor uptake in a CXCR4 expressing

transgenic cell line, [^{64}Cu]AMD3465 was more hydrophilic and showed superior pharmacokinetic properties in comparison to [^{64}Cu]AMD3100, resulting in higher tumor imaging contrast. Both compounds, however, exhibited considerable uptake in the liver and kidneys; the liver uptake has been hypothesized to be partly due to transchelation of ^{64}Cu to liver. Other strategies have been evaluated, whereby AMD3100 and AMD3465 were radiolabeled with ^{68}Ga[17] and ^{11}C,[18] respectively; however, these copper-free approaches showed no improvements in biodistribution *in vivo*. Notably the high liver uptake,[14,18,19] independent of use of radiometal or transchelation, has been assigned in part to the previously reported cytoplasmic and cell-surface expression of CXCR4 protein in liver tissue.[20] Less studied is, however, the role of non-specific transporters - in particular organic cationic transporters (OCTs), given the cationic nature of the cyclam probes - in the liver uptake of the tracers.

Despite the superior properties of ^{18}F-radioisotope, such as low positron energy and adequate half-life (109.7 min), strategies employing this radionuclide for small molecule labeling are limited. A few pyrimidine-based derivatives were labeled with ^{18}F. The small molecule and CXCR4 modulator, MSX-122, was shown to inhibit tumor metastasis and inflammation *in vitro*; however, no *in vivo* imaging evaluation was carried out.[21] Another pyrimidine-pyridine derivative showed no probe accumulation in CXCR4-expressing tumors due to rapid metabolism of the radioligand.[22] Work by Poty *et al.* used AMD3100 analogues as precursors for ^{18}F labeling, but no *in vivo* validation was performed.[23] A structurally similar tracer to AMD3465, [^{18}F]RPS-544, has been evaluated recently.[24] The radioligand showed a moderate uptake in PC3-CXCR4 tumor model and, in addition to substantial uptake in the liver and kidneys, [^{18}F]RPS-544 also accumulated in small and large intestines, differing from the excretion profile of other labeled cyclams.

In this study, we aimed at developing and evaluating a new CXCR4-targeting radioligand that would capitalize on the advantages of ^{18}F, whilst preserving the ability to sensitively detect CXCR4 expression in tumors. Due to the potent binding affinity and selectivity of AMD3465 towards CXCR4, this molecule was chosen as a reference for the development of the tracer, [^{18}F]MCFB.

The most important aspect of the tracer design was high *in vivo* metabolic stability. Pyridines can generally be reacted with [^{18}F]fluoride in the 2 or 4 position to obtain the corresponding labeled fluoropyridines.[25] However, their *in vivo* stability is unpredictable, often resulting in defluorination, with associated uptake of radioactivity in bone.[22,24] Therefore, to facilitate ^{18}F labeling, the 2-pyridylmethylamine moiety was substituted with 1-aminomethyl-4-fluorobenzene. The former was linked to the original 1,4-phenylenebismethylene linker by N-substituted ethylene chain. The introduction of ^{18}F isotope was achieved by using the easily accessible prosthetic group, [^{18}F]fluorobenzaldehyde, which can be further converted into [^{18}F]fluorobenzylamine through reductive amination.[26]

The applicability of [^{18}F]MCFB for sensitive and specific imaging of CXCR4 was evaluated, as well as its *in vivo* pharmacokinetics and biodistribution in relevant tumor models.

MATERIALS AND METHODS

Materials

Unless otherwise indicated, reagents and solvents were purchased from Sigma-Aldrich (Haverhill, UK) and used without further purification. AMD3465 was purchased from Tocris Bioscience (R&D Systems, Abingdon, UK).

4-*N*,*N*,*N*-trimethylammonium benzaldehyde (triflate salt) was synthesized according to a method published in the literature.[27] Flash column chromatography was carried out on silica gel (Aldrich silica gel, pore size 60 Å, particle size 230-400 mesh). Thin layer chromatography (TLC) was performed on Merck Silica 60 F_{254} plates. ^{1}H NMRs, ^{13}C NMRs and ^{19}F NMRs were recorded on a Bruker AV-400 spectrometer at a frequency of 400, 101 and 376 MHz, respectively. Chemical shifts (δ) are given in parts per million (ppm) as referenced to the appropriate residual solvent peaks. Signals are assigned as s, d, m and br for singlet, doublet, multiplet and broad, respectively. ^{13}C NMRs are complicated by existence of C-F coupling (long range including) and conformers. Mass spectra (*m/z*) were obtained in a positive electrospray ionization on a Waters LCT Premier (ES-ToF). Crude reaction mixtures were analyzed by TLC and HPLC.

HPLC Methods (a) Purity analysis of nonradioactive and radioactive compounds was carried out on a Shimadzu Prominence HPLC system equipped with a LC-10Ai pump, a SPD-20A UV detector (λ= 254 nm), a Flow-RAM sodium iodide/PMT gamma detector and a Laura 4.1.1.3 software (LabLogic); Phenomenex Gemini 5µ C18 150 x 4.6 mm and Luna 5µ Phenyl-Hexyl 150 x 4.6 mm columns were used and a mobile phase comprising of Water (0.1%TFA)/MeCN with a gradient of 5% organic for 1 min, 5→95% in 16 min, 95% organic for 2 min, 95→5% organic in 2 min, delivered at a flow rate of 1 mL/min. (b) Semi-preparative radio-HPLC was carried out using a Shimadzu LC-20AT pump, a Bioscan Flowcount FC3200 sodium iodide/PMT gamma detector (LabLogic) and a Knauer UV detector (λ= 254 nm). Sample injection, product isolation and data collection were performed using an in-house build Multi-stream

HPLC system and bespoke software package (Hammersmith Imanet Ltd., UK) and an Agilent 5µ Exlipse XDB-C18 250 × 9.4 mm column with an isocratic mobile phase of Water (0.1%TFA)/MeCN (62:38 v/v) at a flow rate of 3mL/min; injection loop 10 mL. (c) Metabolite analysis was carried out using an Agilent 1100 series G1312A pump and a LabLogic Laura 3 software equipped with a linear G1314A UV detector (λ=254 nm), a γ-RAM model 3 detector and a Phenomenex Luna 5µ Phenyl-Hexyl 250 × 10 mm column with an isocratic mobile phase of Water (0.1%TFA)/MeCN (80:20 v/v) at a flow rate of 3mL/min; injection loop 1 mL.

Synthesis of precursor and reference compound

1,1',1''-(1,4,8,11-tetraazacyclotetradecane-1,4,8-triyl)tris(2,2,2-trifluoroethan-1-one) (1)

To a stirred solution of cyclam (1 g, 4.99 mmol) and triethylamine (0.69 mL, 4.99 mmol) in methanol (10 mL) was added dropwise ethyl trifluoroacetate (2.36 mL, 19.9 mmol). The homogeneous reaction mixture was cooled with an ice-water bath to control the mild exothermic reaction. Stirring was continued under N_2 overnight. Volatiles were removed under reduced pressure. The residue was dissolved in EtOAc and passed through the plug of silica. The solvent was concentrated to give the product as a white foam (2.6 g, 93%). HRMS (ESI) = 489.1549 $(M + H)^+$. Calc. for C_{16} H_{22} N_4 O_3 F_9: 489.1548. ^{1}H NMR (400 MHz, $CDCl_3$): δ 3.91-3.34 (m, 12H), 3.07-2.84 (m, 2H), 2.81-2.50 (m, 2H), 2.40-2.07 (m, 2H), 1.98-1.67 (m, 2H), 1.17-0.60 (bs, 1H). ^{13}C NMR (101 MHz, $CDCl_3$): δ 160.06-154.85 (m, C=O,), 121.77-111.81 (q, CF_3, *J*=288.6 Hz), 52.55-43.85 (m, CH_2-N), 31.74-25.94 (m, CH_2). ^{19}F NMR (376 MHz, $CDCl_3$): δ -63.56 – -72.90 (m).

1,1',1''-(11-(4-(bromomethyl)benzyl)-1,4,8,11-tetraazacyclotetradecane-1,4,8-triyl)tris(2,2,2-trifluoroethan-1-one) (2)

To a stirred solution of **1** (1.95 g, 3.99 mmol) and K_2CO_3 (717 mg, 5.2 mmol) in CH_3CN (70 mL) was added α,α'-dibromo-*p*-xylene (5.25 g, 19.9 mmol) and the reaction mixture stirred at 70°C for 1 h. The solution was cooled to room temperature and the solvent removed under reduced pressure. The residue was partitioned between brine (50 mL) and CH_2Cl_2 (100 mL). The organic phase was separated, dried (Na_2SO_4) and silica added, the mixture was evaporated to dryness. The compound impregnated on silica was purified by flash chromatography (first with CH_2Cl_2, followed by CH_2Cl_2/Ether, 9:1) to give the desired compound as a white solid (1.8 g, 67%). HRMS (ESI) = 671.1273 $(M + H)^+$. Calc. for $C_{24}\ H_{29}\ N_4\ O_3\ Br\ F_9$: 671.1279. ^1H NMR (400 MHz, $CDCl_3$): δ 7.55 – 7.01 (m, 4H), 4.50 (s, 2H), 3.99 – 3.23 (m, 14H), 2.95 – 2.62 (m, 2H), 2.62 – 2.27 (m, 2H), 2.28 – 1.92 (m, 2H), 1.90 – 1.43 (m, 2H). ^{13}C NMR (101 MHz, $CDCl_3$): δ 158.07– 156.48 (m), 138.23 – 136.41 (m), 130.55 – 128.42 (m), 120.99 – 111.59 (m), 61.02 – 58.94 (m), 56.06 – 44.52 (m), 33.30 – 32.47 (m), 29.95 – 23.65 (m). ^{19}F NMR (376 MHz, $CDCl_3$): δ -68.31 – -69.57 (m).

1,1',1''-(11-(4-(((2-aminoethyl)amino)methyl)benzyl)-1,4,8,11-tetraazacyclotetradecane-1,4,8-triyl)tris(2,2,2-trifluoroethan-1-one) (3)

To a stirred solution of ethylenediamine (134 mg, 2.2 mmol) and K_2CO_3 (93 mg, 0.675 mmol) in dry CH_3CN (5 mL) at -10 °C (acetone/ice bath) was added dropwise a solution of 1-[1-methylene-4-(bromo-methylene)phenylene]-4,8,11-tris(trifluoroacetyl)-1,4,8,11-tetra-azacyclotetradecane (**2**) (300 mg, 0.45 mmol) in CH_3CN (20 mL) over 15-20 min. After stirring for a further 30 min, the reaction mixture

was filtered and concentrated to provide a residue which was purified by chromatography on silica gel using 1% TEA in EtOAC:MeOH (7:3) to give the product as a white solid (180 mg, 62%). HRMS (ESI) = 651.2708 $(M + H)^+$. Calc. for $C_{26}H_{36}N_6O_3F_9$: 651.2705. ^{1}H NMR (400 MHz, DMSO-d_6): δ 7.33 – 7.10 (m, 4H), 3.87 – 3.18 (m, 15H), 3.09 – 2.24 (m, 12H), 2.18 – 1.95 (m, 2H), 1.83 – 1.63 (m, 2H). ^{13}C NMR (101 MHz, DMSO-d_6): δ 157.30– 154.95 (m), 141.15 – 139.76 (m), 137.61 – 136.04 (m), 130.23 – 127.12 (m), 121.54 – 111.81 (m), 59.71 – 58.30 (m), 54.43 – 43.32 (m), 41.65 (s), 29.51 – 22.06 (m). ^{19}F NMR (376 MHz, DMSO-d_6): δ -66.66 – -74.74 (m).

1,1',1''-(11-(4-(((2-((4-fluorobenzyl)amino)ethyl)amino)methyl)benzyl)-1,4,8,11-tetraazacyclotetradecane-1,4,8-triyl)tris(2,2,2-trifluoroethan-1-one) (4)

To a stirred solution of the amine **3** (100 mg, 0.153 mmol) in dry CH_3CN (10 mL), at room temperature, were added 4-fluorobenzaldehyde (12.6 μL, 0.118 mmol), and catalytical amount of glacial acetic acid. The resulting solution was stirred at room temperature for 1 h and $NaBH(OAc)_3$ (75 mg, 0.354 mmol) was added. The mixture was left to stir overnight. Acetonitrile was removed under vacuum. The residue was dissolved in EtOAc, washed with saturated aqueous $NaHCO_3$, dried (Na_2SO_4), concentrated, and purified by chromatography on silica gel using 0.5% TEA in EtOAC:MeOH (8:2). The desired product was obtained as a white solid (40 mg, 34%). MS (ESI): *m/z* 759 $[MH^+]$. ^{1}H NMR (400 MHz, DMSO-d_6): δ 7.64 – 6.76 (m, 8H), 3.89 – 3.23 (m, 19H), 3.19 – 2.53 (m, 6H), 2.49 – 2.21 (m, 2H), 2.22 – 1.93 (m, 3H), 1.88-1.60 (m, 2H). ^{13}C NMR (101 MHz, DMSO-d_6): δ 162.68 (s), 160.28 (s), 158.23– 154.29 (m), 140.47 – 139.58 (m), 138.16 – 135.95 (m), 130.84 – 127.03 (m), 121.41 – 111.86 (m), 115.25-115.04 (d, *J*=21.1 Hz), 59.86 – 58.02 (m), 54.38 – 43.14 (m), 52.46 (s),

48.49 (s), 31.53 – 22.35 (m). ^{19}F NMR (376 MHz, DMSO-d_6): δ -67.85 – -68.75 (m), -116.76 (s).

N1-(4-((1,4,8,11-tetraazacyclotetradecan-1-yl)methyl)benzyl)-N2-(4-fluorobenzyl)ethane-1,2-diamine (5)

To a stirred solution of the trifluoroacetyl-protected amine **4** (70 mg, 0.09 mmol) in MeOH (2.0 mL), at room temperature was added 5N NaOH (200 μL). The resulting solution was stirred at room temperature overnight. The solvent was removed under reduced pressure, and CH_2Cl_2 (5 mL) and water (2.0 mL) were added to the residue. The phases were separated, and the aqueous phase was extracted with CH_2Cl_2 (3 × 5 mL). The combined organic phases were washed with 1N NaOH, dried (Na_2SO_4) and concentrated to give a free base (40 mg, 93%). HRMS (ESI) = 471.3609 $(M + H)^+$. Calc. for $C_{27}H_{44}N_6F$: 471.3611. ^{1}H NMR (400 MHz, $CDCl_3$): δ 7.31-7.05 (m, 6H), 7.04-6.82 (m, 2H), 3.67 (s, 4H), 3.48 (s, 2H), 2.85-2.31 (m, 23H), 1.87-1.70 (m, 2H), 1.67-1.51 (m, 2H). ^{13}C NMR (101 MHz, $CDCl_3$): δ 163.07 (s), 160.64 (s), 139.04 (s), 137.47 (s), 136.23 (d, *J*=3.2 Hz), 129.62- 127.86 (m), 115.34-114.84 (d, *J*=21.2 Hz), 57.45 (s), 54.53 (s), 53.67 (s), 53.27 (s), 53.19 (s), 50.83 (s), 49.36 (s), 49.17 (s), 48.97 (s), 48.78 (s), 48.02 (s), 47.41 (s), 28.66 (s), 26.25 (s). ^{19}F NMR (376 MHz, $CDCl_3$): δ -116.25 (s).

Radiosynthesis of [^{18}F]MCFB

The no-carrier-added aqueous [^{18}F]fluoride solution, typically 1.5 mL, 1.4 GBq, was transferred to a FASTlab™ automated synthesis module (GE Healthcare Life Sciences, Amersham, UK). The activity was trapped on a Waters QMA-carbonate Sep-Pak SPE cartridge and eluted into a reaction vessel with 1000 μL of an eluent solution (800 μL of Kryptofix 2.2.2 (6mg/mL in acetonitrile), 200 μL of $KHCO_3$ (3.5mg/mL in

H_2O)). The eluate was evaporated to dryness by a combination of vacuum and nitrogen flow at 120°C for 12 min. After drying, anhydrous acetonitrile (400 μL) was added to a dried residue in the reaction vessel, and the remaining of the radiosynthesis was carried out manually.

To a Wheaton vial containing 2.0 mg of 4-trimethylammonium-benzaldehyde trifluoromethanesulfonate precursor dissolved in acetonitrile (100 μL) dried [^{18}F]fluoride (370-555 MBq in 300 μL acetonitrile) was added at ambient temperature. The labeling reaction was conducted at 90°C for 15 min before allowing it to reach room temperature. A solution of cyclam-amine (6.0 mg) in acetonitrile (100 μL) was then added followed by heating at 50°C for 15 min. Afterwards, reaction mixture was cooled again to ambient temperature and neat sodium triacetoxyborohydride (4.5 mg) was added and heating resumed for 30 min at 50°C. The reaction was quenched by addition of 0.1%TFA in water (10 mL) and purified by semi-preparative radio-HPLC. The fraction of eluent containing **[^{18}F]-4** was collected and diluted to a final volume of 40 mL with water, then immobilized on a Sep Pak tC18 light cartridge (Waters) [pre-conditioned with acetonitrile (5 mL) and water (10 mL)]. The cartridge was then washed with water (5 mL) followed by elution of the radioligand using ethanol (300 μL). To a solution of ethanol was added 1M NaOH (200 μL) and the mixture was left at room temperature for 15 min. Formulation was achieved by addition of 1M HCl to provide [^{18}F]MCFB.

Radiochemical purity was confirmed by co-elution with a reference compound (**Supplementary Figure 1**).

LogD determination

Briefly, 7 MBq of the ligand in 20 μL of phosphate buffered saline (PBS) was added to a mixture of 2 mL of n-octanol and 2 mL of PBS, pH 7.4; the n-octanol was washed with PBS before use. The mixture was vigorously shaken for 1 h at room temperature and then centrifuged at 5000 rpm for 5 min; 100 μL aliquots from each of the two phases were drawn and their radioactivity content was measured in a γ-counter (LKB Wallac 1282 Compugamma laboratory gamma counter, PerkinElmer, Massachusetts, USA). The n-octanol/PBS partition coefficient was determined by dividing the radioactivity found in the n-octanol layer by that found in the PBS layer. The $LogD_{Octanol/PBS}$ value is reported as the average of three independent experiments.

Cell culture

The human triple-negative metastatic breast cancer cell lines MDA-MB-231-luc, MDA-MB-231 shSC, and MDA-MB-231 shCXCR4, the CXCR4-overexpressing glioma cell line U87.CD4.CXCR4, as well as the diffuse large B-cell lymphoma cell lines U2932 and SuDHL8 were cultured in Roswell Park Memorial Institute (RPMI) Medium (Sigma-Aldrich). MDA-MB-231-luc (hitherto referred to as MDA-MB-231) is a luciferase-expressing wild-type MDA-MB-231 cell line obtained from PerkinElmer (Waltham, MA, USA). CXCR4 expression was silenced by doxycycline-inducible shRNA targeting CXCR4 (pTRIPZ CXCR4 shRNA clone V3THS_346208; Dharmacon, Lafayette, USA) to obtain MDA-MB-231 shCXCR4, or non-targeting shRNA (Dharmacon) to obtain MDA-MB-231 shSC. Viruses were packaged using Trans-Lentiviral shRNA Packaging System (Dharmacon). Stable clones were FACS sorted based on the expression of a doxycycline-inducible TurboRFP reporter gene

within the same construct. CXCR4 knockdown was induced by incubation with doxycycline-hyclate (Sigma-Aldrich) for indicated times. All cell lines were cultured in the presence of 10% Fetal Bovine Serum (FBS) (Sigma-Aldrich), 2mM L-glutamine (Invitrogen, Carlsbad, USA) and 100 U/mL penicillin-streptomycin (Invitrogen) in a humidified atmosphere of 5% CO_2 at 37°C.

[^{125}I]SDF-1 ligand binding assay

The [^{125}I]SDF-1 ligand binding to CXCR4 on U87.CD4.CXCR4 cells and antagonism by [^{19}F]MCFB was conducted as previously described by us.[28] AMD3465 was used as positive control.

***In vitro* radioligand uptake**

Cells were seeded in 6-well plates at a density of 400,000-600,000 cells/well 24h prior to the experiment. For blocking studies, U2932 and SuDHL8 cells were treated with vehicle or 500 μg/mL AMD3465 for 5 min before addition of radioactivity. For knockdown studies, MDA-MB-231 shCXCR4 or relevant shSC control cells were treated with doxycycline at a concentration of 0.5 μg/mL for 24 h prior to uptake studies. In hypoxia studies, cells were placed within a filtered hypoxia chamber (Oxoid Anaerojar, Thermo Fisher Scientific) that achieves < 1% O_2, and incubated at 37°C, 5% CO_2 (balance N_2) for 16 h. Cells evaluated under normoxic conditions were incubated in 21% O_2, 5% CO_2 and balance N_2 for 16 h at 37°C.

Cells were then incubated with radioligand at 0.74 MBq/well for 60 min at 37°C, under 5% CO_2. Following incubation, cells were placed on ice, and washed 3 times with ice-cold PBS. After washing, cells were lysed with RIPA buffer (Sigma-Aldrich) for 5 min. The radioactivity of the lysate was measured by γ-counting. Counts/min data

were expressed as a percentage of the incubated dose (ID) of radioactivity in each well and total cellular protein concentration of the sample, determined using Pierce® BCA assay (Thermo Fisher Scientific), i.e., %ID/mg protein.

***In vitro* internalization studies**

For internalization experiments, MDA-MB-231 cells were plated in 6-well plates at a density of 600 000 cells/well and allowed to recover for 24 h at 5% CO_2, at 37°C. On the day of the assay, cells were incubated with approximately 0.74 MBq/well of [^{18}F]MCFB for 30 min at 4°C (assuming inhibition of receptor internalization at this temperature) or at 37°C. In conditions incubated at 4°C, the media was replaced with fresh 37°C media and incubated for 5, 15, 30 and 60 min at 37°C. After incubation, surface-bound radioactivity was removed by washing the cells with 400 µL of ice-cold 50 mM glycine in 150 mM NaCl (pH=3) for 5 min on ice, followed by two washes with ice-cold PBS. To obtain the internalized fraction, cells were lysed with 400 µL of 1M of NaOH. The radioactivity of the internalized fraction was measured by γ-counting. Counts/min data were expressed as a percentage of the incubated dose (ID) of radioactivity in each well and total cellular protein concentration of the sample, determined using Pierce® BCA assay, i.e., %ID/mg protein. The percentage of internalization was calculated as:

$$Internalization(\%) = \frac{internalized\ fraction}{surface\ bound\ fraction + internalized\ fraction} \times 100$$

Immunoblotting

For western blot analysis, cells (80-90% confluency) were placed on ice, the medium was removed, and cells were washed 3 times with ice-cold PBS and lysed with RIPA buffer supplemented with 100X Pierce™ protease and phosphatase inhibitor cocktail (Thermo Fisher Scientific) for 10 min on ice. Whole lysates were sonicated, and total protein concentration was quantified using the Pierce™ BCA protein assay kit (Thermo Fisher Scientific). Lysates were mixed with NuPage® LDS loading buffer and reducing agent (Invitrogen), and denatured at 70°C for 10 min. Equal amounts of protein (30 µg) were resolved on 4-15% Mini-PROTEAN® TGX™ gels (Bio-Rad, Hemel Hempstead, UK) and separated by gel electrophoresis at 290V for 15 min. The gels were then transferred to PVDF membranes (Trans-Blot Turbo Transfer Packs, Bio-Rad) using the Trans-Blot® Turbo™ System (Bio-rad). Membranes were blocked for 1 h in 5% milk in PBS containing 0.1% v/v Tween® 20 (Sigma-Aldrich) (PBST) and incubated with rabbit anti-human CXCR4 clone UMB2 (1:1000; ab124824, Abcam), Danvers, USA), and mouse anti-HIF-1α clone 54 (1:1000; BD Biosciences, USA) overnight at 4°C. After washing with PBST, goat anti-rabbit Immunoglobin G (IgG) horseradish peroxidase (IgG-HRP) (1:2000, SC-2004, Santa Cruz Biotechnology, Dallas, USA) or goat anti-mouse lgG-HRP (1:2000, SC-2005, Santa Cruz Biotechnology) were incubated in 5% milk-TBST for 1 hour at room temperature. Signals were detected using Amersham enhanced chemiluminescence (ECL) Plus Western Blotting Detection Reagent kit (GE Healthcare Life Sciences) and Amersham Hyper-film (GE Healthcare Life Sciences). Intensity of protein bands was normalized to β-actin (mouse anti-β –actin antibody (1:10,000, ab6276, Abcam)) and analyzed using ImageJ version 1.44h (National Institutes of Health).

Immunofluorescence

For immunofluorescence staining of tumor CXCR4 expression, formalin-fixed paraffin embedded tumor slices (of 5 μm thickness) were stained with rabbit anti-CXCR4 UMB2 clone antibody (1:200) in blocking buffer overnight at 4°C. The slides were subsequently washed with PBST thrice and incubated with Alexa Fluor® 488 goat anti-rabbit IgG secondary antibody (1:400; Molecular Probes™, Thermo Fisher Scientific) in blocking buffer for 1 h at room temperature, protected from light. Following another washing step, the slides were mounted using ProLong® gold antifade reagent with 4'-6-diamidino-2-phenylindole (DAPI) (Life Technologies Ltd., Thermo Fisher Scientific). Immunofluorescence imaging was performed using a 40X or 60X UPlanAPO objective lens on an Olympus BX-51 wide-field microscopy UIS2 optical system (Olympus Life Science Europa GMBH, Hamburg, Germany) equipped with a DP70 digital camera. Images were acquired using an Olympus U-RFL-T epifluorescence source and DPController 1.2.1.108 imaging software (Olympus Optical Co. Ltd, Tokyo, Japan) in the red, blue and green channels. Image processing was performed using ImageJ version 1.44h.

***In vivo* radioligand uptake**

All animal experiments were done by licensed investigators in accordance with the UK Home Office Guidance on the Operation of the Animal (Scientific Procedures) Act 1986 (HMSO, London, UK, 1990) and within guidelines set out by the UK National Cancer Research Institute Committee on Welfare of Animals in Cancer Research.[29]

The *in vivo* models were established in female athymic nude mice (MDA-MB-231 tumor model) or in NOD/SCID mice (U2932 and SuDHL8 tumor models) aged 6 to 8 weeks (Harlan, Bicester, UK Ltd). Xenografts were established under 2.5% isoflurane

anaesthesia by subcutaneous injection of MDA-MB-231 cell line ($5x10^6$ cells in 100 μL PBS) or U2932 and SuDHL8 ($5x10^6$ cells in 100 μL of 50% PBS and 50% Matrigel (Corning, Amsterdam, The Netherlands)) in the back of the neck of the mice. Tumor dimensions were measured by caliper and volumes calculated using the ellipsoid formula that is best for estimating tumor mass: Volume (mm^3) = (π/6) x a x b x c, where a, b and c represent 3 orthogonal axes of the tumor. Mice were used for imaging when tumor volume reached approximately 100 mm^3 (at approximately 4-6 weeks post-induction).

For imaging, mice were anesthetized with 2.5% isoflurane and placed in a thermostatically controlled rig in a dedicated small animal Genisys^4 PET scanner (SOFIE Biosciences, Culver City, USA). Following injection of 0.925 MBq of [^{18}F]MCFB *via* lateral tail vein cannula, PET scans were acquired in a list-mode format over either 0-60 min (dynamic scan) or 40-60 min after injection (static scan) to give decay-corrected values of radioactivity accumulation in tissues. The collected data were ordered into 6 (dynamic scan) or 2 (static scan) time frames of 600 seconds and reconstructed with a 3-dimensional maximum likelihood estimation method (3D ML-EM). Volumes of interest (VOIs) for tumors and different organs were defined using Siemens Inveon Research Workplace software (Siemens Molecular Imaging Inc., Knoxville, USA) and the count densities (MBq/mL) of these VOIs were averaged for the time points corresponding to 40-60 min (where equilibrium was observed). Tissue radioactivity uptake values were normalized to whole-body uptake, a method used in previous publications.[30–32]

Metabolism Studies

Non-tumor-bearing were injected intravenously with 3.7 MBq of [^{18}F]MCFB. Plasma, urine and liver were collected at the indicated time and were snap-frozen in liquid nitrogen for subsequent HPLC analysis. For extraction, ice cold CH_3CN (1.0 mL) was added to plasma. The mixture was centrifuged (15,493 x g, 4°C, 3 min) and the resulting supernatant was evaporated to dryness under vacuum at 40°C using a rotary evaporator. Liver samples were diced and homogenized with ice cold CH_3CN (1.0 mL) using Precellys® 24 homogenizer prior to centrifugation. The supernatant was then decanted and evaporated to dryness. The samples were resuspended in HPLC mobile phase (1.2 mL) and filtered through a 13 mm Pall Acrodisc syringe filter (0.2 μm). The samples were analyzed by radio-HPLC.

Biodistribution Studies

Biodistribution studies were carried out 60 min after injection of 0.925 MBq of [^{18}F]MCFB *via* lateral tail vein cannula. Tissue samples were quickly collected, and radioactivity content was determined by γ-counting and normalized to sample weight. Treatment with metformin hydrochloride (Sigma-Aldrich) was carried out by injection of 50 mg/kg of metformin intravenously in U2932-bearing mice 30 min prior injection of radioactivity. The dose of metformin selected was based on the work by Wilcock and Bailey[33] that indicates that a 50 mg/kg bolus is equivalent to the maximum recommended daily dosage in humans.

Statistics

Data were expressed as mean ± SEM. Statistical analysis was done using unpaired 2-tailed Student's t-test or two-way ANOVA with Bonferroni correction as appropriate

and defined as significant (*, 0.01<p<0.05), very significant (**, 0.001<p<0.01) and extremely significant (***, p<0.001).

RESULTS

Non-radioactive synthesis of precursor 3 and reference compound 5

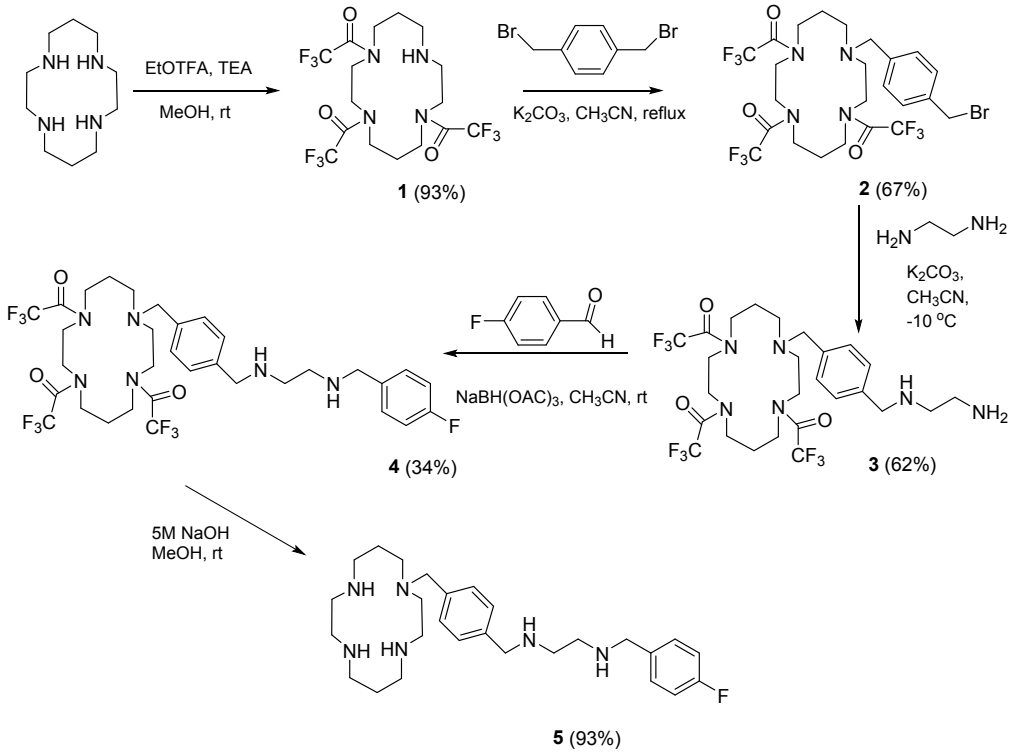

Scheme 1. Synthesis of compound **5** from cyclam.

The synthesis of precursor **3** and reference compound **5** is shown in (**Scheme 1**). The protection of cyclam with EtOTFA was done using previously optimized conditions with triethylamine.[34] The subsequent *N*-alkylation of the tri-protected cyclam **1** with α, α'-dibromo-p-xylene using K_2CO_3 in acetonitrile gave the desired bromomethyl

intermediate **2** in 67% isolated yield. Initial attempts to alkylate ethylenediamine with intermediate **2** at elevated temperature unfortunately increased formation of by-products, which were subsequently minimized by performing the reaction at -10°C and using an excess of the diamine to give a 62% yield. Additionally, the precursor **3** was further used for the preparation of reference compound **5**. First, the compound **4** was prepared by the reductive amination of 4-fluorobenzaldehyde with **3** using $NaBH(OAc)_3$ in acetonitrile. Straight-forward mild deprotection of the amides *via* MeOH in aqueous NaOH afforded free base within 16 hours in a yield of 93%.

Radiochemistry and Partition Coefficient

The labeled variant of **5** was prepared *via* a three-step procedure: a) radiosynthesis of the ^{18}F-labeling prosthetic group 4-[^{18}F]fluorobenzaldehyde ([^{18}F]FBA), followed by b) reductive amination and c) global deprotection. [^{18}F]FBA was synthesized from 4-*N*,*N*,*N*-trimethylammonium benzaldehyde (triflate salt) *via* a standard fluorination route (K[^{18}F]F/Kryptofix 222) in acetonitrile at 90°C for 15 min and was used for the next step without further purification (**Scheme 2A**). Substitution of potassium carbonate for the less basic potassium hydrogen carbonate improved reproducibility of the reaction significantly, most likely due to the higher stability of the precursor under these conditions (as seen by the UV trace from analytical HPLC of the incorporation). The average radiochemical incorporation as measured by analytical radio-HPLC was >95%.

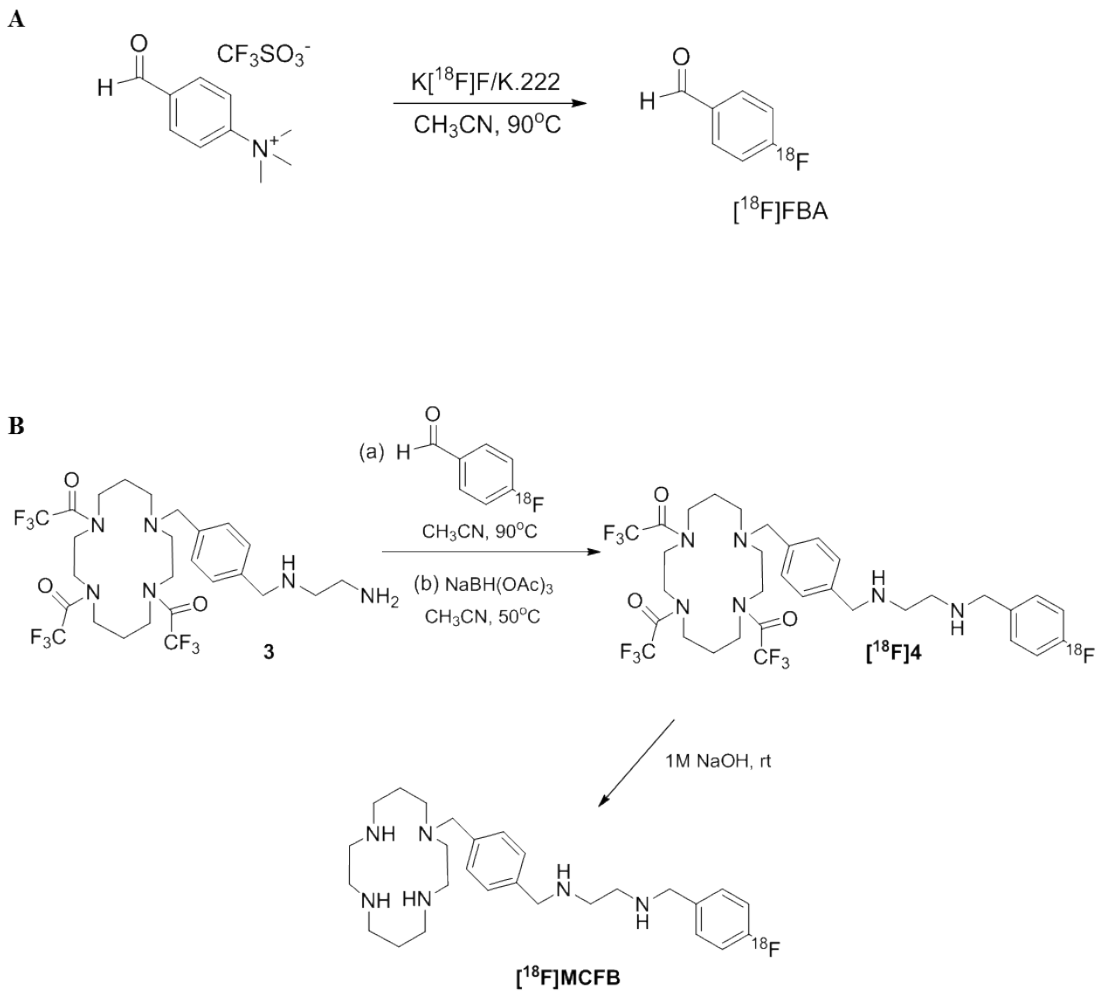

Scheme 2. Radiosynthesis of [^{18}F]MCFB. **A.** Synthesis of [^{18}F]FBA. **B.** Synthesis of [^{18}F]MCFB from precursor **3** using [^{18}F]FBA.

The subsequent step was the reductive alkylation of amine **3** with the intermediate [^{18}F]FBA using $NaBH(OAc)_3$ as the reducing agent (**Scheme 2B**). The reaction was performed as one-pot two-step synthesis. Parameters such as temperature, solvent, reaction time and sequence of reagent addition were investigated. The optimal conditions were found to be 15 min reaction time for the initial formation of the imine (which was not isolated) and a further 30 min for subsequent reduction with $NaBH(OAc)_3$. The solvent of choice for both steps was acetonitrile, with the reaction carried out at 50°C to produce the alkylated amine **[^{18}F]4**.

Finally, deprotection of **[^{18}F]4** was carried out using 1M NaOH at room temperature affording the desired molecule [^{18}F]MCFB with complete conversion within 10 min. As the procedure was carried out manually with low amounts of radioactivity, only a modest specific activity (5.7 GBq/μmol) was achieved. The radiosynthetic procedure from ^{18}F fluoride including formulation of [^{18}F]MCFB took 2.5 h in total. Overall, the decay-corrected yield of 14.1 ± 2.5 % (n=5) was achieved.

The $LogD_{Octanol/PBS}$ of [^{18}F]MCFB was found to be -1.64 ± 0.06.

Competitive Binding, Receptor Expression and Internalization of [^{18}F]MCFB

Binding of [^{19}F]MCFB to CXCR4 was estimated from its inhibitory effect on binding of the native ligand CXCL12 to CXCR4 in cells. [^{19}F]MCFB or AMD3465 (positive control) inhibited CXCL12-CXCR4 interaction in a concentration-dependent manner (**Supplementary Figure 2**). The 50% inhibitory values (IC_{50}) for [^{19}F]MCFB and AMD3465 were 111.3 ± 4.0 and 89.8 ± 3.5 nM, respectively.

For *in vitro* binding studies, we used a highly-expressing native CXCR4 B-cell lymphoma cell line, U2932, and compared it against another B-cell lymphoma cell line with lower CXCR4 expression, SuDHL8.[35] The [^{18}F]MCFB uptake was higher in U2932 cell line (0.86 ± 0.15%ID/mg) than in SuDHL8 (0.52 ± 0.05%ID/mg) and co-incubation with AMD3465 resulted in partial inhibition of tracer binding (37% for U2932 and 45% for SuDHL8). The difference in tracer uptake between cell lines was smaller than the variation of CXCR4 protein expression (96% difference of CXCR4/β-actin) (**Figure 2A**), and together with the partial blocking of tracer uptake after AMD3465 treatment, suggests some level of non-specific binding.

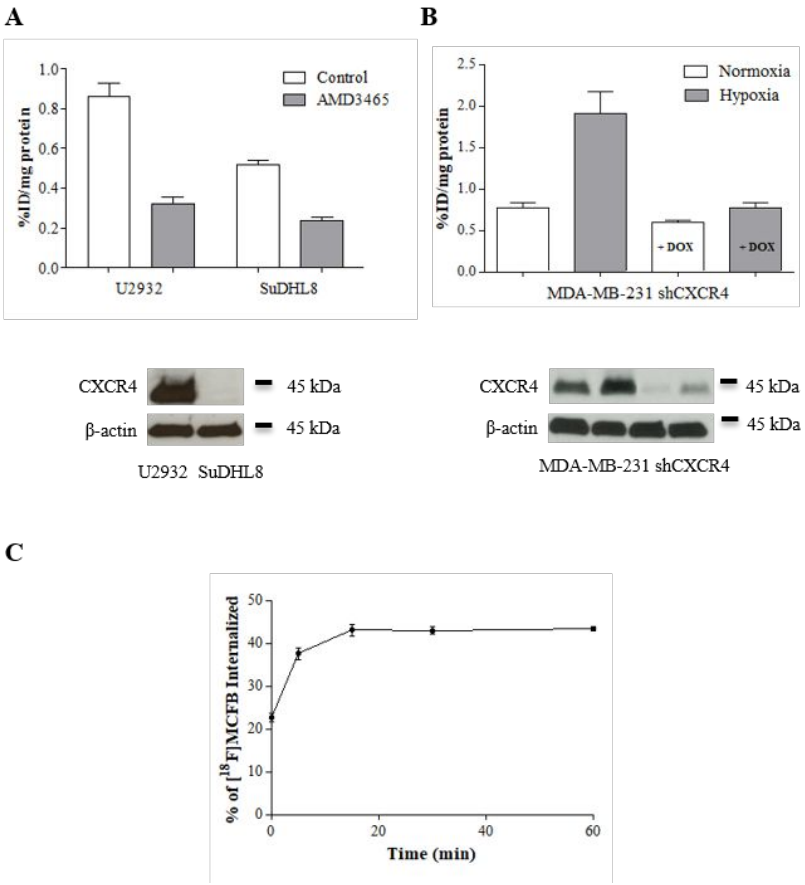

Figure 2. *In vitro* characterization of [^{18}F]MCFB. **A.** Uptake of [^{18}F]MCFB normalized to cellular protein in U2932 and SuDHL8 cell lines, with or without blocking for 5 min with AMD3465. **B.** Effect of CXCR4 knockdown on [^{18}F]MCFB radioactive uptake. MDA-MB-231 cells transduced with a doxycycline-inducible CXCR4-targeted (shCXCR4) short hairpin RNA construct were incubated under normoxia or hypoxia (< 1% O_2 for 16 h) in the presence or absence of doxycycline (0.5 mg/ml for 24 h). Typical western blots of CXCR4 expression (and β-actin for loading control) in U2932, SuDHL8 and MDA-MB-231 shCXCR4 cell lines are shown below. **C.** Internalization of [^{18}F]MCFB in MDA-MB-231 cell line. All data are mean ± SEM, n=6.

Specific uptake of [^{18}F]MCFB was further confirmed by the use of isogenic MDA-MB-231 cells transduced with a doxycycline-inducible CXCR4-targeted shRNA

(shCXCR4). Tracer accumulation was 2-fold higher in hypoxia-induced cells compared to normoxic conditions, in accordance with the higher CXCR4 expression (**Figure 2B**). Hypoxia induction was confirmed by HIF-1α expression (**Supplementary Figure 3**). Receptor knockdown in the MDA-MB-231 shCXCR4 cell line by treatment with doxycycline resulted in reduced tracer uptake, again demonstrating [^{18}F]MCFB sensitivity for CXCR4 expression. In the control MDA-MB-231 shSC cell line, cellular uptake of [^{18}F]MCFB was unperturbed by the doxycycline treatment, as expected (**Supplementary Figure 4**). To determine uptake mechanism, we incubated MDA-MB-231 cells with [^{18}F]MCFB at 4°C, subsequently transitioning them to 37°C. [^{18}F]MCFB was rapidly internalized, with the internal fraction reaching 40% of the total uptake within the first 15 min (**Figure 2C**). Indeed, at 37°C, the internalized fraction was 9.8 ± 0.9%ID/mg, whereas at 4°C, only 2.9 ± 0.3%ID/mg was found intracellularly (**Supplementary Figure 5**), pointing to the role of internalization as part of tracer uptake mechanism.

PET Imaging

Subsequently, we investigated tracer accumulation in mice bearing U2932 and SuDHL8 tumors, together with a non-transgenic variant of MDA-MB-231. Representative PET images show high [^{18}F]MCFB accumulation in the tumor models at 60 min post-radioligand injection (**Figure 3A**). Uptake was 2-fold higher in U2932 (T/WB ratio 4 ± 0.8) than in SuDHL8 (T/WB ratio 2.1 ± 0.3) and MDA-MB-231 (T/WB ratio 1.6 ± 0.1) (**Figure 3B**). Interestingly, the signal uptake (U2932 > SuDHL8 > MDA-MB-231) was not in accordance with expression of CXCR4 (U2932 > MDA-MB-231 > SuDHL8).

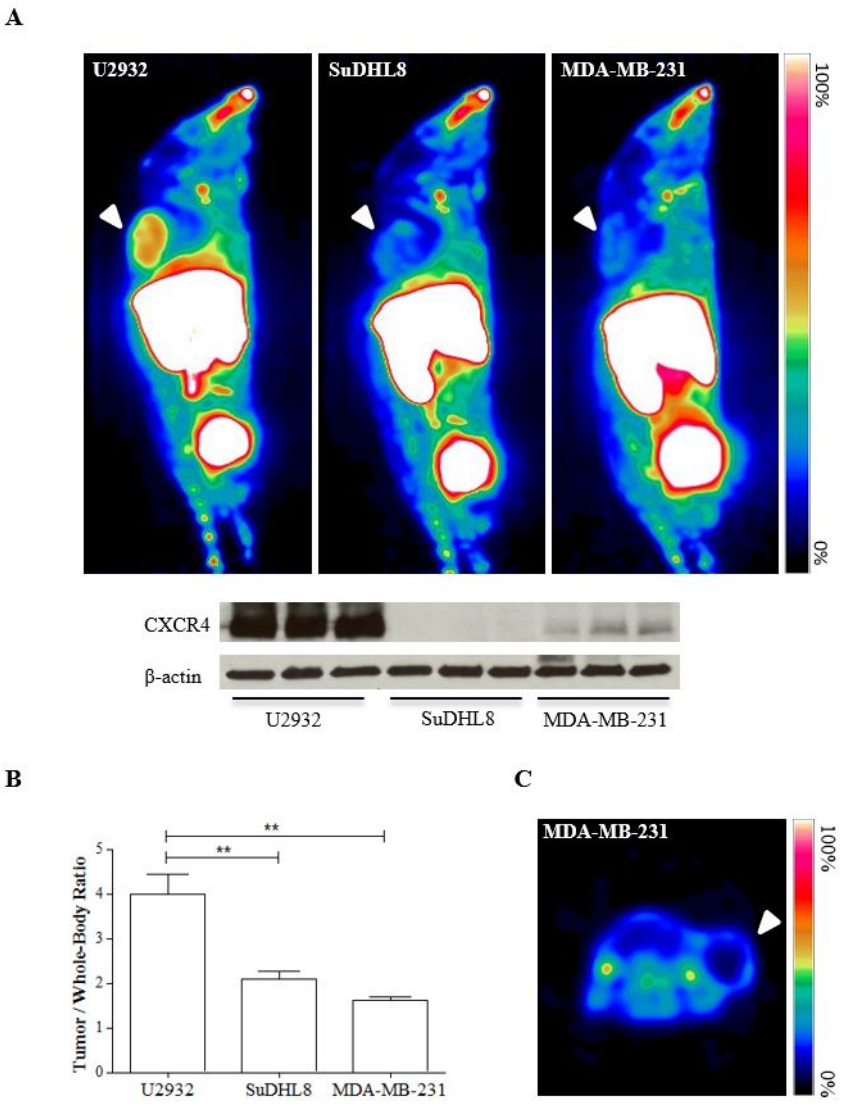

Figure 3. [^{18}F]MCFB discriminates differential CXCR4 expression *in vivo*. **A.** Representative sagittal [^{18}F]MCFB-PET images derived from summed 60 min dynamic scans in U2932, SuDHL8 and MDA-MB-231 xenograft-bearing mice. CXCR4 expression in excised tumors was determined by western blot (results shown for 3 independent samples per tumor model). **B.** Quantification of [^{18}F]MCFB uptake in the different tumor models by region of interest analysis normalized to whole-body radioactivity. Data are mean ± SEM, n=4. **C.** Representative axial [^{18}F]MCFB-PET image of a MDA-MB-231 xenograft-bearing mouse where necrosis is visible. White arrows indicate tumors.

This mismatch may be due to the central necrotic areas identified in the MDA-MB-231 tumors (**Figure 3C**). This phenotype has been described for this tumor model[36] and the compromised vasculature can significantly reduce tracer delivery, not only to the necrotic core but also to the surrounding tissue. Thus, receptor binding in the whole tumor is likely to be affected, hindering differences in uptake between treatment groups as was evident in our work. High tracer uptake was also seen in liver, bladder and the snout region. Immunofluorescent staining of the excised tumors showed expression of CXCR4 in both cell lymphoma lines (**Figure 4A**), although significantly higher in the U2932 compared to the SuDHL8 ($p<0.001$) (**Figure 4B**).

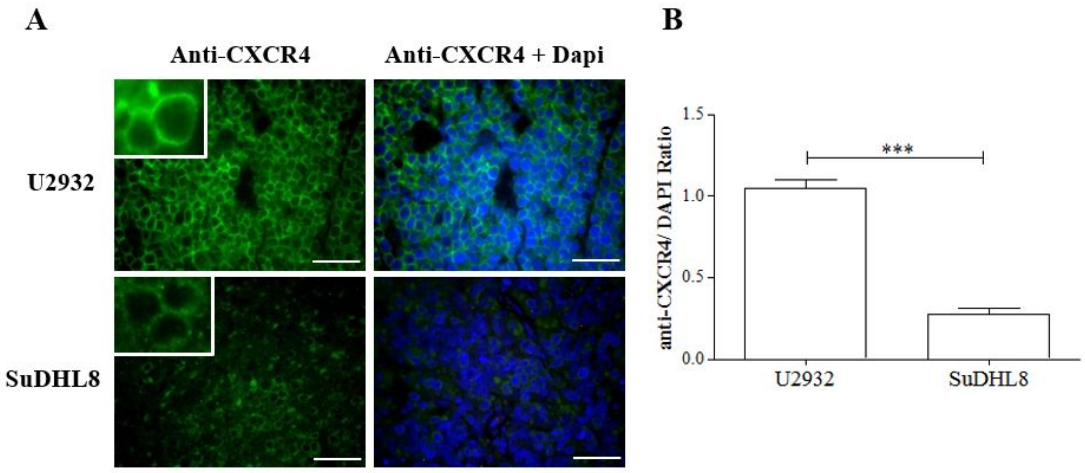

Figure 4. A. Representative images of excised tumor tissues stained by immunofluorescence for CXCR4 (green) and DAPI (blue). **B.** Quantification of CXCR4-fluorescence intensity normalized to DAPI.

[^{18}F]MCFB Biodistribution

Biodistribution was carried out in U2932 and SuDHL8 tumor-bearing mice 60 min after injection of [^{18}F]MCFB (**Figure 5A**). Tumor uptake was 3.3 ± 0.9%ID/g for U2932 tumors, and 1.81 ± 0.04%ID/g for SuDHL8 tumors. The low levels of bone uptake for both SuDHL8 and U2932-bearing mice (1.6 ± 0.3%ID/g and 1.4 ± 0.2%ID/g, respectively) suggest that tracer defluorination did not ensue upon intravenous injection, and renal elimination occurred as indicated by the high tracer localization in kidneys (42.1 ± 1.8%ID/g and 43.1 ± 7.3%ID/g, respectively) and urine (521.7 ± 178.5%ID/g and 688.8 ± 50.4%ID/g, respectively). High [^{18}F]MCFB accumulation in the liver was also seen (51.9 ± 2.9%ID/g for SuDHL8 and 63 ± 4.9%ID/g for U2932-bearing mice).

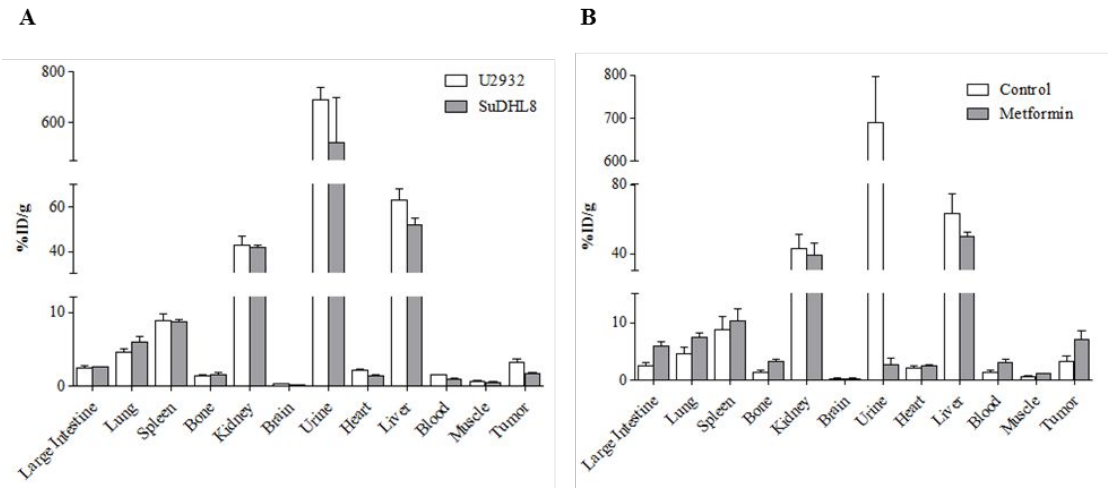

Figure 5. Biodistribution of [^{18}F]MCFB. **A.** Mice bearing U2932 and SuDHL8 xenografts **B.** Mice bearing U2932 treated with 50 mg/kg of metformin for 30 min were injected with 1.48 MBq of [^{18}F]MCFB and tissues were excised 60 minutes after injection. Radioactivity in the tissues was counted and is expressed as fraction of injected dose normalized to tissue weight. Data are mean ± SEM, n=4.

Radio-chromatographic analysis of plasma and liver extracts obtained at 15 or 60 min after [^{18}F]MCFB injection showed only parent compound indicating good *in vivo* metabolic stability (**Supplementary Figure 6**) suggesting that the high liver uptake was unlikely due to metabolism. Similarly to AMD3465, [^{18}F]MCFB has a positive charge at physiological pH. We hypothesized that polyspecific transporters, such as the organic cation transporter 1 (OCT1), 2 (OCT2) and 3 (OCT3), may be involved in the transport of the tracer into the metabolic organs. To test this hypothesis, we treated U2932 tumor-bearing mice with 50 mg/kg of metformin, an oral insulin-sensitizing drug that is a substrate for OCT1, OCT2 and OCT3, and imaged the mice with [^{18}F]MCFB (**Figure 5B and Supplementary Figure 7**). Biodistribution studies showed a marked decrease in urinary excretion of [^{18}F]MCFB after metformin treatment (688.8 ± 50.4% to 2.8 ± 0.4%ID/mg), and moderate decrease in the kidneys and liver; all the other organs showed small increases in [^{18}F]MCFB uptake.

DISCUSSION

We report the development of the ^{18}F cyclam-based radioligand, [^{18}F]MCFB, designed for sensitive detection of CXCR4. Several PET-dedicated tracers have been developed for the imaging of CXCR4 by exploiting modifications of therapeutically relevant antagonists to accommodate different radioisotopes. Cyclam-based tracers, such as AMD3100 and AMD3465, have shown promising characteristics for CXCR4 imaging; however, they have also been plagued with high hepatic accumulation. Given that CXCR4 is expressed in the liver, some degree of specific liver uptake is expected. Most strategies employ ^{64}Cu for the radiolabeling of cyclams, whose structures accommodate metals without the need of a chelator. However, ^{64}Cu is known to

undergo transchelation[37] and could contribute to non-specific uptake in the liver. This is supported by previous work with the ^{18}F-radiolabeled T140 peptide that showed significantly lower accumulation in the liver compared to its analogous radiometal chelates.[7,8] From the foregoing, we designed a new monocyclam ligand to incorporate an ^{18}F radiolabel, to exploit the physical properties of ^{18}F and potentially improve *in vivo* biodistribution. This work describes the synthesis and preclinical evaluation of the resulting tracer, [^{18}F]MCFB.

Mutational mapping and molecular modelling showed that the amino groups of these cyclams are important in binding to CXCR4 *via* electrostatic interactions between the positively charged nitrogens and the negatively charged carboxylates present within CXCR4 protein. [^{18}F]MCFB was designed based on the AMD3465 structure; the minimum number of nitrogen atoms required to achieve sufficient interaction with the CXCR4 active binding site through hydrogen-bonding was preserved.[38] Thus, antagonism for SDF-1-CXCR4 interaction by [^{19}F]MCFB was not compromised: the IC_{50} of [^{19}F]MCFB (111.3 nM) for CXCR4 was comparable to that of AMD3465 (89.8 nM).

Our results showed that the cellular uptake of [^{18}F]MCFB was sensitive to modulation of CXCR4 expression within the same cellular background: knockdown of CXCR4 with shRNA decreased [^{18}F]MCFB uptake, whereas hypoxia increased radioligand uptake, consistent with differences in CXCR4 expression. Furthermore, the tracer was able to differentiate between two cell lines, U2932 and SuDHL8, with different CXCR4 expression *in vitro*, and uptake was inhibited in the presence of AMD3465. The observation that uptake in U2932 and SuDHL8 did not reflect the difference in CXCR4 expression indicates a degree of non-specific binding of the radiotracer.

Consistent with its negative $LogD_{Octanol/PBS}$, studies in MDA-MB-231 showed that [^{18}F]MCFB was rapidly internalized and remained inside the cell, in a similar fashion to [^{64}Cu]AMD3465[19] and *N*-[^{11}C]methyl-AMD3465.[18] We have shown that CXCR4 is also expressed in the intracellular compartments of MDA-MB-231 (**Supplementary Figure 8**), thus radiotracer binding to cytosolic proteins, following possible release from internalized CXCR4 in cells for instance, could potentially result in retention and higher signal-to-noise ratio. It therefore appears that the non-specific binding of [^{18}F]MCFB to cells does not result from defective internalization. Furthermore, surface expression of the analogous receptor that shares binding to SDF-1, CXCR7, occurred at low but equivalent levels in both U2932 and SuDHL8 cells (**Supplementary Figure 9**), thus, does not explain non-specific binding.

Based on 60-min dynamic PET data, we performed quantification of [^{18}F]MCFB *in vivo* at 40-60 min post tracer injection. [^{18}F]MCFB showed sufficiently high tumor-to-background localization to permit tumor detection. As with the *in vitro* studies, the difference in tracer uptake was disproportionate to differences in CXCR4 protein expression between U2932 and SuDHL8 by western blot *in vivo*; this could be the result of limitations of the western blot technique, as it can only provide relative measurements. Indeed, immunofluorescence staining of excised specimens showed low but detectable CXCR4 expression in the SuDHL8 tumors, in accordance to existing literature.[35]

In vivo biodistribution of [^{18}F]MCFB showed high uptake in organs with high levels of CXCR4, such as liver, lung and spleen, similarly to the profile reported for CXCR4-based PET tracers.[18,19] The accumulation of [^{18}F]MCFB in CXCR4 expressing tumor tissue derived from naturally-occurring models was only modest (3.3 and 1.81%ID/g for U2932 and SuDHL8, respectively), but similar to the uptake of [^{18}F]RPS-544 in a

CXCR4-overexpressing model (3.4 ± 1.2%ID/g in PC3-CXCR4 tumors).[24] Although it would be reasonable to expect more uptake of radioligand in transgenic cells than in naturally derived cells, head-to-head comparison of [^{18}F]MCFB and previously reported radiolabeled cyclams is challenging owed to the use of models with vastly different CXCR4 profiles.

High radioactivity accumulation in the urine and kidneys indicate that elimination of [^{18}F]MCFB occurred *via* the urinary system. The uptake of [^{18}F]MCFB in the liver was similar to other AMD3465-based imaging agents (liver-to-muscle ratio of 74, 86 and 150 for [^{18}F]MCFB, [^{64}Cu]AMD3465 and *N*-[^{11}C]methyl-AMD3465, respectively). The clearance of [^{18}F]MCFB differed from [^{18}F]RPS-544, which showed high uptake in small and large intestine; the excretion of [^{18}F]MCFB was more similar to non-fluorine containing cyclam based radioligands reported in the literature.

Metabolite analysis of [^{18}F]MCFB from mouse plasma, urine and liver (tissues excised 1h p.i.) by radio-HPLC showed only the presence of parent compound (**Supplementary Figure 6**). However, it should be noted that extraction efficiency was not measured, thus any insoluble metabolites or adducts formed between the parent and liver would not have been detected by the method used. Bone uptake was found to be low suggesting that defluorination was negligible or absent; this was expected as defluorination of fluorinated arenes is uncommon.

The liver plays an essential role in removing drugs or toxins from circulation in the human body, as well as in the clearance of various endogenous compounds.[39] At physiological pH, several compounds are positively charged, thus requiring transport proteins to facilitate crossing the plasma membrane into the hepatocytes. Organic cation transporters (OCTs) mediate the uptake of a wide variety of these compounds; OCT1, expressed primarily in the liver, is particularly important in the hepatic elimination of

numerous small molecules.[40] At physiological pH, both AMD3100 and AMD3465 have a positive charge, owing to the charged nitrogens in the cyclam moieties.[41] Similarly, [^{18}F]MCFB has a positive charge, which led us to hypothesize that it may be a substrate for OCTs. Metformin is a substrate for OCT1, which has been reported as the primary hepatic transporter for this drug.[42] Pre-dosing with metformin led to a small decrease in [^{18}F]MCFB uptake in the liver, which, together with the increased radioactivity in the blood, suggests some level of competitive inhibition of OCT1 (and perhaps OCT3) in this organ. A marked decrease in urinary excretion of [^{18}F]MCFB suggests involvement of these polyspecific transporters in the renal elimination of the tracer. Interestingly, the decrease of [^{18}F]MCFB uptake in urine was not reflected in the kidney. OCT2 is important for the renal clearance of metformin, and its subsequent excretion into urine.[43] Given the rapid clearance of metformin, we speculate that competitive inhibition of [^{18}F]MCFB kinetics by metformin is only transient, with partial restoration of OCT2 over time such that by 60 min - the time point in biodistribution studies - the localization of [^{18}F]MCFB in the kidneys of metformin-treated mice is not significantly different from that of metformin-naïve mice. In contrast, urine radioactivity reflects the cumulative elimination of radioactivity over the entire 60 min period and more accurately reflects kidney function, compared to kidney [^{18}F]MCFB-derived radioactivity at any one time point. This is consistent with previously reported results, whereby [^{11}C]-labeled metformin was co-injected with unlabeled metformin; the authors showed decreased urinary clearance in the presence of unlabeled metformin, in agreement with a pharmacokinetic profile showing higher kidney radioactivity at very early time points and becoming similar at 60 min, i.e. higher kidney exposure in the untreated tumors concordant with higher urine levels.[44]

However, this work is only a preliminary study, and the extent of transport inhibition would need to be assessed with a range of metformin concentrations.

Further work in well-defined CXCR4 non-expressing cells (e.g., via CRISPR) is also required to verify if various OCTs contribute to the non-specific binding of [^{18}F]MCFB in tumor cells.

Overall, these data suggest that the high liver uptake seen with cyclam-based tracers is likely to be influenced by a variety of mechanisms; besides CXCR4-mediated uptake and transchelation of radiometals (not relevant to ^{11}C or ^{18}F candidates), the high overall positive charge [^{18}F]MCFB, required for CXCR4 receptor interaction, may also contribute to non-specific interaction, as recently described by others for similar cyclams.[45] Of note, this is not due to lipophilicity as the measured $LogD_{Octanol/PBS}$ was in the negative range – which also precludes it from passing blood brain barrier (BBB). Therefore, the radioligand appears unsuitable for imaging both brain (without a compromised BBB) and liver lesions, but adequate for use in non-abdominal anatomical locations, though more work would be necessary to optimize the pharmacokinetics for use in abdominal regions *in vivo*.

CONCLUSIONS

We report the design, synthesis and biological testing of a novel and promising ^{18}F-radiolabeled cyclam, [^{18}F]MCFB, for PET imaging of CXCR4 expression. [^{18}F]MCFB showed CXCR4-dependent specific and sensitive uptake, though some non-specific binding was also seen. *In vivo* imaging demonstrated that this tracer is capable of tumor detection and CXCR4 characterization in models with naturally-occurring receptor expression. Elevated hepatic uptake complicates detection of liver metastases, but it is

in conformity with other cyclam-based PET agents. Nonetheless, [^{18}F]MCFB showed potential as a CXCR4-targeting tracer.

ASSOCIATED CONTENT

Supporting Information

Material and Methods for Immunofluorescence and Flow Cytometry; Affinity of [^{19}F]MCFB for the CXCR4 receptor; Confirmation of hypoxia induction by HIF-1α protein expression analysis; *In vitro* uptake of [^{18}F]MCFB in the control cell line MDA-MB-231 shSC; *In vivo* stability of [^{18}F]MCFB in mouse plasma, urine and liver; Subcellular localization of CXCR4; Expression of CXCR7 in U2932 and SuDHL8 cell lines determined by flow cytometry.

AUTHOR INFORMATION

Corresponding Authors

*Eric Aboagye: e.aboagye@imperial.ac.uk. Tel.: + 44 (0)20 3313 3759

ACKNOWLEDGMENT

This work was funded by Cancer Research UK-Engineering and Physical Sciences Research Council (in association with the Medical Research Council and Department of Health (England)) grant C2536/A10337 and Cancer Research UK grant C2536/A16584. EOA acknowledges support from Imperial College NIHR Biomedical Research Centre award (WSCC_P62585), Medical Research Council grant (MC-A652-

5PY80), and Experimental Cancer Medicine Centres grant (C37/A7283). We thank Dr. Louis Allott for all his help and support throughout the writing of this manuscript.

COMPETING INTERESTS

The authors declare no competing interest.

REFERENCES

1. Teicher B, Fricker S. CXCL12 (SDF-1)/CXCR4 pathway in cancer. *Clin Cancer Res*. 2010;16(11):2927-2931. doi:10.1158/1078-0432.CCR-09-2329.

2. Domanska UM, Kruizinga RC, Nagengast WB, et al. A review on CXCR4/CXCL12 axis in oncology: No place to hide. *Eur J Cancer*. 2013;49(1):219-230. doi:10.1016/j.ejca.2012.05.005.

3. Müller A, Homey B, Soto H, et al. Involvement of chemokine receptors in breast cancer metastasis. *Nature*. 2001;410(6824):50-56. doi:10.1038/35065016.

4. Burger JA, Kipps TJ. CXCR4: a key receptor in the crosstalk between tumor cells and their microenvironment. *Blood*. 2006;107(5):1761-1767. doi:10.1182/blood-2005-08-3182.

5. Kopp H-G, Ramos CA, Rafii S. Contribution of endothelial progenitors and proangiogenic hematopoietic cells to vascularization of tumor and ischemic tissue. *Curr Opin Hematol*. 2006;13(3):175-181. doi:10.1097/01.moh.0000219664.26528.da.

6. Shi J, Wei Y, Xia J, et al. CXCL12–CXCR4 contributes to the implication of bone marrow in cancer metastasis. *Futur Oncol*. 2014;10(5):749-759. doi:10.2217/fon.13.193.

7. Jacobson O, Weiss ID, Kiesewetter DO, Farber JM, Chen X. PET of tumor CXCR4 expression with 4-18F-T140. *J Nucl Med*. 2010;51(11):1796-1804. doi:10.2967/jnumed.110.079418.

8. Jacobson O, Weiss ID, Szajek LP, et al. PET imaging of CXCR4 using copper-64 labeled peptide antagonist. *Theranostics*. 2011;1:251-262.

9. Jacobson O, Weiss ID, Szajek LP, et al. Improvement of CXCR4 tracer specificity for PET imaging. *J Control Release*. 2012;157(2):216-223. doi:10.1016/j.jconrel.2011.09.076.

10. Gourni E, Demmer O, Schottelius M, et al. PET of CXCR4 expression by a (68)Ga-labeled highly specific targeted contrast agent. *J Nucl Med*. 2011;52(11):1803-1810. doi:10.2967/jnumed.111.098798.

11. Demmer O, Gourni E, Schumacher U, Kessler H, Wester H-J. PET Imaging of CXCR4

Receptors in Cancer by a New Optimized Ligand. *ChemMedChem*. 2011;6(10):1789-1791. doi:10.1002/cmdc.201100320.

12. Debnath B, Xu S, Grande F, Garofalo A, Neamati N. Small Molecule Inhibitors of CXCR4. *Theranostics*. 2013;3(1):47-75. doi:10.7150/thno.5376.

13. Jacobson O, Weiss ID, Szajek L, Farber JM, Kiesewetter DO. 64Cu-AMD3100—A novel imaging agent for targeting chemokine receptor CXCR4. *Bioorg Med Chem*. 2009;17(4):1486-1493. doi:10.1016/j.bmc.2009.01.014.

14. Nimmagadda S, Pullambhatla M, Stone K, Green G, Bhujwalla ZM, Pomper MG. Molecular imaging of CXCR4 receptor expression in human cancer xenografts with [64Cu]AMD3100 positron emission tomography. *Cancer Res*. 2010;70(10):3935-3944. doi:10.1158/0008-5472.CAN-09-4396.

15. De Silva R a, Peyre K, Pullambhatla M, Fox JJ, Pomper MG, Nimmagadda S. Imaging CXCR4 expression in human cancer xenografts: evaluation of monocyclam 64Cu-AMD3465. *J Nucl Med*. 2011;52(6):986-993. doi:10.2967/jnumed.110.085613.

16. Woodard LE, De Silva RA, Behnam Azad B, et al. Bridged cyclams as imaging agents for chemokine receptor 4 (CXCR4). *Nucl Med Biol*. 2014;41(7):552-561. doi:10.1016/j.nucmedbio.2014.04.081.

17. Poty S, Gourni E, Désogère P, et al. AMD3100: A Versatile Platform for CXCR4 Targeting 68Ga-Based Radiopharmaceuticals. *Bioconjug Chem*. 2016;27(3):752-761. doi:10.1021/acs.bioconjchem.5b00689.

18. Hartimath S V, van Waarde a, Dierckx R a JO, de Vries EFJ. Evaluation of N-[(11)C]methyl-AMD3465 as a PET tracer for imaging of CXCR4 receptor expression in a C6 glioma tumor model. *Mol Pharm*. 2014;11(11):3810-3817. doi:10.1021/mp500398r.

19. De Silva RA, Peyre K, Pullambhatla M, Fox JJ, Pomper MG, Nimmagadda S. Imaging CXCR4 Expression in Human Cancer Xenografts: Evaluation of Monocyclam 64Cu-AMD3465. *J Nucl Med*. 2011;52(6):986-993. doi:10.2967/jnumed.110.085613.

20. Shibuta K, Mori M, Shimoda K, Inoue H, Mitra P, Barnard GF. Regional expression of CXCL12/CXCR4 in liver and hepatocellular carcinoma and cell-cycle variation during in vitro differentiation. *Jpn J Cancer Res*. 2002;93(7):789-797.

21. Liang Z, Zhan W, Zhu A, et al. Development of a Unique Small Molecule Modulator

of CXCR4. Yang P-C, ed. *PLoS One*. 2012;7(4):e34038. doi:10.1371/journal.pone.0034038.

22. Demoin DW, Shindo M, Zhang H, et al. Synthesis and evaluation of an 18F-labeled pyrimidine-pyridine amine for targeting CXCR4 receptors in gliomas. *Nucl Med Biol*. 2016;43(10):606-611. doi:10.1016/J.NUCMEDBIO.2016.05.005.

23. Poty S, Désogère P, Goze C, et al. New AMD3100 derivatives for CXCR4 chemokine receptor targeted molecular imaging studies: synthesis, anti-HIV-1 evaluation and binding affinities. *Dalt Trans*. 2015;44(11):5004-5016. doi:10.1039/C4DT02972K.

24. Amor-Coarasa A, Kelly J, Ponnala S, et al. [18F]RPS-544: A PET tracer for imaging the chemokine receptor CXCR4. *Nucl Med Biol*. 2018;60:37-44. doi:10.1016/J.NUCMEDBIO.2018.01.004.

25. Dollé F. Fluorine-18-labelled fluoropyridines: advances in radiopharmaceutical design. *Curr Pharm Des*. 2005;11(25):3221-3235.

26. Wilson AA, Dannals RF, Ravert HT, Wagner HN. Reductive amination of [18F]fluorobenzaldehydes: Radiosyntheses of [2-18F]- and [4-18F]fluorodexetimides. *J Label Compd Radiopharm*. 1990;28(10):1189-1199. doi:10.1002/jlcr.2580281012.

27. Chang YS, Jeong JM, Lee YS, et al. Preparation of 18F-human serum albumin: A simple and efficient protein labeling method with 18F using a hydrazone-formation method. *Bioconjug Chem*. 2005;16(5):1329-1333. doi:10.1021/bc050086r.

28. George GPC, Stevens E, Åberg O, et al. Preclinical evaluation of a CXCR4-specific (68)Ga-labelled TN14003 derivative for cancer PET imaging. *Bioorg Med Chem*. 2014;22(2):796-803. doi:10.1016/j.bmc.2013.12.012.

29. Workman P, Aboagye EO, Balkwill F, et al. Guidelines for the welfare and use of animals in cancer research. *Br J Cancer*. 2010;102(11):1555-1577. doi:10.1038/sj.bjc.6605642.

30. Nguyen Q-D, Smith G, Glaser M, Perumal M, Arstad E, Aboagye EO. Positron emission tomography imaging of drug-induced tumor apoptosis with a caspase-3/7 specific [18F]-labeled isatin sulfonamide. *Proc Natl Acad Sci*. 2009;106(38):16375-16380. doi:10.1073/pnas.0901310106.

31. Witney TH, Pisaneschi F, Alam IS, et al. Preclinical evaluation of 3-18F-fluoro-2,2-dimethylpropionic acid as an imaging agent for tumor detection. *J Nucl Med*.

2014;55(9):1506-1512. doi:10.2967/jnumed.114.140343.

32. Evans HL, Nguyen Q-D, Carroll LS, et al. A bioorthogonal 68Ga-labelling strategy for rapid in vivo imaging. *Chem Commun*. 2014;50(67):9557-9560. doi:10.1039/C4CC03903C.

33. Wilcock C, Bailey CJ. Accumulation of metformin by tissues of the normal and diabetic mouse. *Xenobiotica*. 1994;24(1):49-57. doi:10.3109/00498259409043220.

34. Yang W, Giandomenico CM, Sartori M, Moore DA. Facile N-1 protection of cyclam, cyclen and 1,4,7-triazacyclononane. *Tetrahedron Lett*. 2003;44(12):2481-2483. doi:10.1016/S0040-4039(03)00338-1.

35. Wester HJ, Keller U, Schottelius M, et al. Disclosing the CXCR4 expression in lymphoproliferative diseases by targeted molecular imaging. *Theranostics*. 2015;5(6):618-630. doi:10.7150/thno.11251.

36. Nofiele JT, Cheng H-LM, Hart G, Shilkaitis A, Gupta T Das. Establishment of a Lung Metastatic Breast Tumor Xenograft Model in Nude Rats. Sun L-Z, ed. *PLoS One*. 2014;9(5):e97950. doi:10.1371/journal.pone.0097950.

37. Buck E. Rogers †,#, Carolyn J. Anderson *,†, Judith M. Connett ‡, et al. Comparison of Four Bifunctional Chelates for Radiolabeling Monoclonal Antibodies with Copper Radioisotopes: Biodistribution and Metabolism. 1996. doi:10.1021/BC9600372.

38. Hatse S, Princen K, De Clercq E, et al. AMD3465, a monomacrocyclic CXCR4 antagonist and potent HIV entry inhibitor. doi:10.1016/j.bcp.2005.05.035.

39. Coleman MD. *Human Drug Metabolism : An Introduction*. Wiley-Blackwell; 2010.

40. Boxberger KH, Hagenbuch B, Lampe JN. Common drugs inhibit human organic cation transporter 1 (OCT1)-mediated neurotransmitter uptake. *Drug Metab Dispos*. 2014;42(6):990-995. doi:10.1124/dmd.113.055095.

41. De Clercq E. The bicyclam AMD3100 story. *Nat Rev Drug Discov*. 2003;2(7):581-587. doi:10.1038/nrd1134.

42. Chen L, Shu Y, Liang X, et al. OCT1 is a high-capacity thiamine transporter that regulates hepatic steatosis and is a target of metformin. *Proc Natl Acad Sci U S A*. 2014;111(27):9983-9988. doi:10.1073/pnas.1314939111.

43. Chen Y, Li S, Brown C, et al. Effect of genetic variation in the organic cation transporter

2 on the renal elimination of metformin. *Pharmacogenet Genomics*. 2009;19(7):497-504. doi:10.1097/FPC.0b013e32832cc7e9.

44. Jakobsen S, Busk M, Jensen JB, et al. A PET Tracer For Renal Organic Cation Transporters, 11 C-metformin: Radiosynthesis and Preclinical Proof-of-Concept Studies. *J Nucl Med*. 2016. doi:10.2967/jnumed.115.169292.

45. Frindel M, Camus N, Rauscher A, et al. Radiolabeling of HTE1PA: A new monopicolinate cyclam derivative for Cu-64 phenotypic imaging. In vitro and in vivo stability studies in mice. *Nucl Med Biol*. 2014;41:e49-e57. doi:10.1016/j.nucmedbio.2013.12.009.

Abstract Graphics – For Table of Contents Only

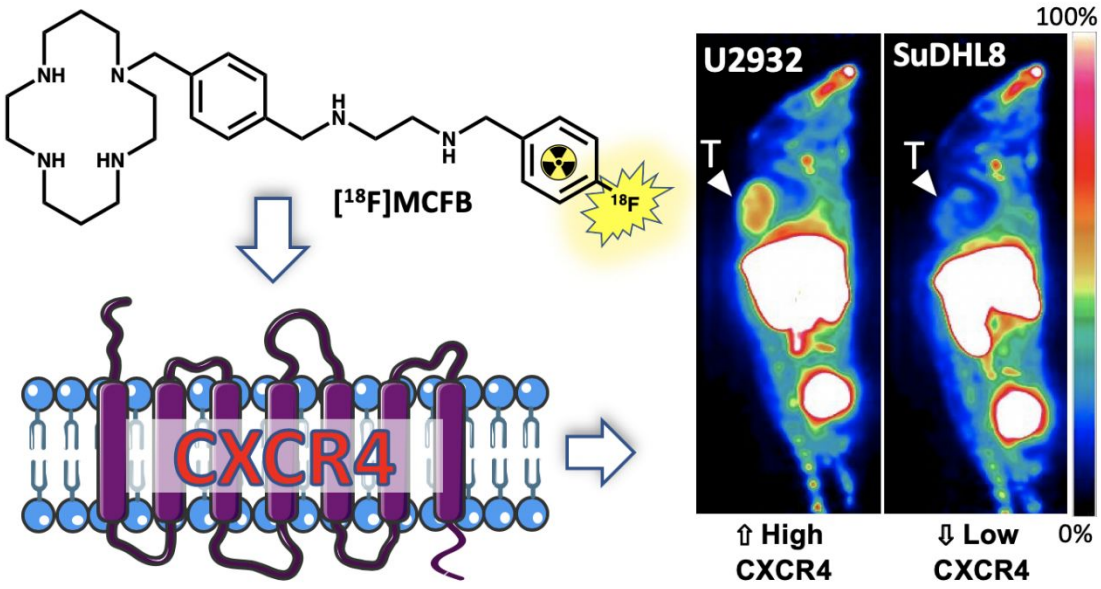
NH
N
NH
HN
H
N
N
H
[18F]MCFB
18F
CXCR4
100%
U2932
SuDHL8
T
T
⇧ High
CXCR4
⇩ Low
CXCR4
0%

1

2

3

4

5

6